Available online at www.sciencedirect.com
ScienceDirect
Journal of Sound and Vibration 303 (2007) 171–184
JOURNAL OF SOUND AND VIBRATION
www.elsevier.com/locate/jsvi

Analytical 3-D *p*-element for quadrilateral plates—Part 1: Thick isotropic plate structures

B. Zhu[a], A.Y.T. Leung[b,*], Q.S. Li[b], J.W.Z. Lu[b], X.C. Zhang[b]

[a]*Department of Civil Engineering, Zhejiang University, China*
[b]*Department of Building and Construction, City University of Hong Kong, Tatchee Avenue, Hong Kong, China*

Received 21 August 2006; received in revised form 5 January 2007; accepted 5 January 2007
Available online 7 March 2007

Abstract

An analytical three-dimensional (3-D) *p*-version element for the vibration analysis of arbitrary quadrilateral thick plates is presented. With the additional hierarchical shape functions and analytically integrated element matrices, the computed accuracy is considerably improved. The computed natural frequencies of cantilever and simply supported square plates show that the convergence rate of the present element is very fast with respect to the number of hierarchical terms and it can predict very accurate modes. The element is applicable to the free vibration analysis of quadrilateral, polygonal plates as well as 3-D space structures. The continuous wavelet transform (CWT) is applied for the identification of damping ratios. Based on the Rayleigh damping model, the damped vibration response is obtained. A simple experiment is performed to verify the predicted vibration responses. The results show that the proposed element is also efficient for the vibration response analysis of plates.

1. Introduction

The finite-element method is one of the most widely used methods for the vibration analysis. For the simulation of actual state of thick plates, three-dimensional (3-D) elements are superior to the ones based on the classical plate theory [1–3], first-order shear deformation plate theory [4] and high-order shear deformation plate theory [5].

Either refining the finite-element mesh or increasing the order of the shape functions can improve the accuracy of finite-element solutions. The former is called *h*-version and the latter *p*-version. It is well known that *p* convergence is more rapid than *h* convergence using the same number of degrees of freedom (DOFs) [6]. The existing 3-D *p*-version elements for the vibration of plates are limited to the analysis of plates with certain shapes [7,8]. It is best that analytical integration is adopted in *p*-version elements [1–4,7,8] or the numerical integration errors will dominate the computed results due to the highly oscillatory nature of the higher-order polynomials involved so that the monotonic convergence of the predicted natural frequencies cannot be

*Corresponding author. Tel.: +852 2788 7600; fax: +852 2788 9643, +852 2788 7612.
E-mail address: Andrew.leung@cityu.edu.hk (A.Y.T. Leung).

0022-460X/$ - see front matter © 2007 Elsevier Ltd. All rights reserved.
doi:10.1016/j.jsv.2007.01.002

Nomenclature

E	Young's modulus
R	circumscribing radius
ρ	mass per unit volume
v	Poisson's ratio
ω	natural frequency
λ, Ω	non-dimensional frequency parameters
p_x, p_y, p_z	number of additional hierarchical terms in three coordinates
x, y, z	Cartesian coordinates
ξ, η, ζ	coordinates in mapped cube
x_i, y_i, z_i	values of x, y and z coordinates at the eight corner nodes
$\mathbf{J}$	Jacobian matrix
$\mathbf{u}$	vector of u, v and w
$\mathbf{K}^e, \mathbf{M}^e$	stiffness matrix and mass matrix of the element

guaranteed [9]. This paper overcomes the problem by analytical integration and presents a new 3-D hierarchical arbitrary quadrilateral element for the vibration analysis of plates.

Some numerical examples including the vibration of square, quadrilateral, polygonal plates and a 3-D space structure are studied in this paper. Comparison with the available methods shows that the present element predicts natural modes with higher accuracy and its convergence rate is very fast with respect to the number of hierarchical terms. The vibration responses computed by the present element are validated by an experiment. The element can be extended to study tapered plates without difficulty.

2. Element formulation

2.1. Stiffness and mass matrices

The coordinates system for a 3-D quadrilateral uniform plate element is shown in Fig 1. Fig 1(a) depicts the Cartesian coordinates of the element, and Fig. 1(b) describes the mapped $\xi-\eta-\zeta$ cube region. The Jacobian matrix is defined in terms of the Cartesian coordinates at the eight corner nodes as

$$J=\begin{bmatrix}\frac{\partial x}{\partial \xi} & \frac{\partial y}{\partial \xi} & \frac{\partial z}{\partial \xi}\\ \frac{\partial x}{\partial \eta} & \frac{\partial y}{\partial \eta} & \frac{\partial z}{\partial \eta}\\ \frac{\partial x}{\partial \zeta} & \frac{\partial y}{\partial \zeta} & \frac{\partial z}{\partial \zeta}\end{bmatrix}=\begin{bmatrix}a+b\eta & d+e\eta & 0\\ c+b\xi & f+e\xi & 0\\ 0 & 0 & t/2\end{bmatrix}, \tag{1}$$

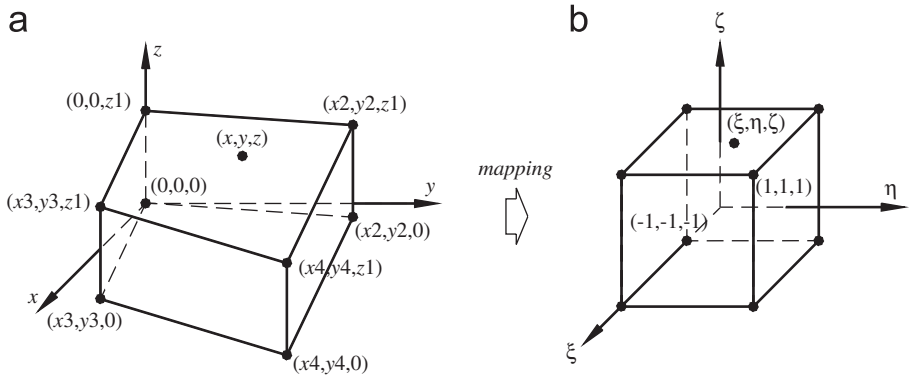

Fig. 1. The 3-D element coordinate transformation.

where $a = 0.25(-x_2 + x_3 + x_4)$, $b = 0.25(-x_2 - x_3 + x_4)$, $c = 0.25(x_2 - x_3 + x_4)$, $d = 0.25(-y_2 + y_3 + y_4)$, $e = 0.25(-y_2 - y_3 + y_4)$, $f = 0.25(y_2 - y_3 + y_4)$ and $t = z_1$. Then the determinant of Jacobian is $|\mathbf{J}| = (t/2)[(ae - bd)\xi + (bf - ce)\eta + af - cd]$, and

$$\mathbf{J}^{-1} = \frac{1}{|\mathbf{J}|}\begin{bmatrix} (f + e\xi)t/2 & -(d + e\eta)t/2 & 0 \\ -(c + b\xi)t/2 & -(a + b\eta)t/2 & 0 \\ 0 & 0 & 2|\mathbf{J}|/t \end{bmatrix}. \tag{2}$$

The displacements u, v and w in the three directions are interpolated by

$$\mathbf{u} = \begin{Bmatrix} u \\ v \\ w \end{Bmatrix} = [\mathbf{N}_1, \mathbf{N}_2, \ldots, \mathbf{N}_i, \ldots, \mathbf{N}_{(p_x+2)(p_y+2)(p_z+2)}] = \mathbf{N}\boldsymbol{\delta}^e, \tag{3}$$

where $\boldsymbol{\delta}^e$ is the vector of the generalized DOFs; parameters p_x, p_y and p_z, respectively, are the numbers of additional hierarchical terms employed in each coordinate axis; and

$$\mathbf{N}_i = \begin{bmatrix} f_j(\xi)f_k(\eta)f_l(\zeta) & 0 & 0 \\ 0 & f_j(\xi)f_k(\eta)f_l(\zeta) & 0 \\ 0 & 0 & f_j(\xi)f_k(\eta)f_l(\zeta) \end{bmatrix}, \tag{4}$$

with $f_j(\xi)$, $f_k(\eta)$ and $f_l(\zeta)$ being the Legendre orthogonal polynomials [1], $j = 1 \sim p_x + 2$, $k = 1 \sim p_y + 2$ and $l = 1 \sim p_z + 2$. The eight shape functions $f_j(\xi)f_k(\eta)f_l(\zeta)$ (j, k, $l = 1$ or 2) are used in the conventional linear finite elements (LFE). The additional shape functions in terms of the Legendre orthogonal polynomials lead to zero displacements at each corner node. With these enriching functions, the additional DOFs appear along the 12 edges, on the six surfaces and in the interior of the element. The DOFs of the eight corner nodes are represented by j, k, $l \leqslant 2$; the DOFs along the 12 edges are represented if one of j, k, $l > 2$; the DOFs on the six surfaces are represented if two of j, k, $l > 2$; the DOFs in the interior are represented if all of j, k, $l > 2$.

The substitution of Eq. (4) into the strain equations gives

$$\boldsymbol{\varepsilon} = \begin{bmatrix} \partial/\partial x & 0 & 0 \\ 0 & \partial/\partial y & 0 \\ 0 & 0 & \partial/\partial z \\ \partial/\partial y & \partial/\partial x & 0 \\ 0 & \partial/\partial z & \partial/\partial y \\ \partial/\partial z & 0 & \partial/\partial x \end{bmatrix} \mathbf{u} = \mathbf{B}\delta^e. \tag{5}$$

In view of the coordinate mapping, the partial derivatives in $\mathbf{B}$ must be replaced by

$$\begin{Bmatrix} \partial/\partial x \\ \partial/\partial y \\ \partial/\partial z \end{Bmatrix} = \mathbf{J}^{-1}\begin{Bmatrix} \partial/\partial \xi \\ \partial/\partial \eta \\ \partial/\partial \zeta \end{Bmatrix}. \tag{6}$$

For harmonic vibration problems, the stiffness matrix and the mass matrix of the element are obtained by applying the principle of minimum potential energy and Hamilton's principle respectively as

$$\mathbf{K}^e = \int_V \mathbf{B}^{\mathrm{T}}\mathbf{D}\mathbf{B}\,\mathrm{d}V = \int_{-1}^{1}\int_{-1}^{1}\int_{-1}^{1} \mathbf{B}^{\mathrm{T}}\mathbf{D}\mathbf{B}|\mathbf{J}|\,\mathrm{d}\xi\,\mathrm{d}\eta\,\mathrm{d}\zeta, \tag{7a}$$

$$\mathbf{M}^e = \int_V \rho\mathbf{N}^{\mathrm{T}}\mathbf{N}\,\mathrm{d}V = \int_{-1}^{1}\int_{-1}^{1}\int_{-1}^{1} \rho\mathbf{N}^{\mathrm{T}}\mathbf{N}|\mathbf{J}|\,\mathrm{d}\xi\,\mathrm{d}\eta\,\mathrm{d}\zeta, \tag{7b}$$

where $\mathbf{D}$ is the 3-D modulus matrix and ρ is the density. The coefficients of the stiffness matrix and the mass matrix are obtained in a straightforward manner and they are given in Appendix A. In the assemblage of

elements, since there are DOFs along every edge and surface of the p-version element, the direction of the edges and surfaces between adjacent elements should be in the same orientation to ensure the continuity along the edges and surfaces. Then, for the eigenvalue problem of free vibration of the structure one has

$$(\mathbf{K}-\omega^2\mathbf{M})\boldsymbol{\delta}=0, \tag{8}$$

where $\mathbf{K}$, $\mathbf{M}$ and $\boldsymbol{\delta}$, respectively, are the global stiffness matrix, global mass matrix and the eigenvector of the structure, and ω is the natural frequency of the structure. For engineering applications when only first several natural frequencies are needed, the internal DOFs and some DOFs not adjacent to other elements can be condensed by the exact dynamic condensation before assembling the elements [10].

2.2. Integration implementation

As mentioned above, it is well known that numerical integration errors influence the results computed by p-version elements and the problem becomes obvious for highly oscillating shape functions such as the higher-order Legendre orthogonal polynomials. Numerical integration softens the stiffness of the elements in general and that the monotonic convergence of the predicted natural frequencies cannot be guaranteed [9]. Numerical quadrature should only be used to predict several lowest frequencies with a few hierarchical terms [11]. The problems will be eliminated if the matrices of the element are integrated analytically. Based on this viewpoint, the p-version elements with analytical integration are always recommended. For the present element, as shown in Appendix A, the problem of integrating the coefficients of stiffness and mass matrices reduces to the integration of $\xi^i\eta^j/(A\xi+B\eta+C)$ with A, B and C being constants. Using some commercial packages such as *MAPLE*, *MATLAB*, *MATCAD* and *MATHEMATICA*, the exact formula of the above integration can be obtained. For example

$$\begin{aligned}\int_{-1}^{1}\int_{-1}^{1}\xi\eta^2/(A\xi+B\eta+C)\,\mathrm{d}\xi\,\mathrm{d}\eta=\frac{1}{12A^2B^3}\{&12AB^3-4ABC^2-12A^3B\\&-\log(A+B+C)[-3A^4+3B^4+C^4-6A^2C^2-8A^3C+4B^3C]\\&-\log(-A+B+C)[3A^4-3B^4-C^4+6A^2C^2-8A^3C-4B^3C]\\&-\log(A-B+C)[3A^4-3B^4-C^4+6A^2C^2+8A^3C+4B^3C]\\&-\log(-A-B+C)[-3A^4+3B^4+C^4-6A^2C^2+8A^3C-4B^3C]\}.\end{aligned} \tag{9}$$

To use these integration formulae with different values of i and j conveniently, one can make them into a function for formulating the stiffness and mass matrices of the element. By this way, the coefficients of the stiffness matrix and the mass matrix are readily obtained in a straightforward manner.

3. Numerical results

Some combinations of free (F), simply supported (S) and clamped (C) boundary conditions are considered in this paper. All DOFs at the free surface and the clamped surface are unconstrain and constrain, respectively. The simply supported condition presumes unconstrain DOFs at the side surface and zero transverse and tangential displacements at the common edge between the side surface and the nether surface of the plate. Unless stated otherwise, the Poisson's ratio v is taken to be 0.3. To simplify the computation and presentation, the numbers of the additional hierarchical terms in the three dimensions are taken as a common value, that is, $p_x=p_y=p_z=p$.

3.1. Vibration analysis of square plates

In order to examine the accuracy and convergence rate of solutions computed by the 3-D hierarchical finite-element method (HFEM) for free vibration of thick plates, a cantilever square plate with $t/a=0.5$ is meshed by one square (mesh I), four squares (mesh II) and four quadrilaterals (mesh III) present 3-D p-version elements, respectively (see Fig. 2). The frequency parameters $\lambda=(\omega a^2/\pi^2)\sqrt{\rho t/D_0}$ of the first eight modes

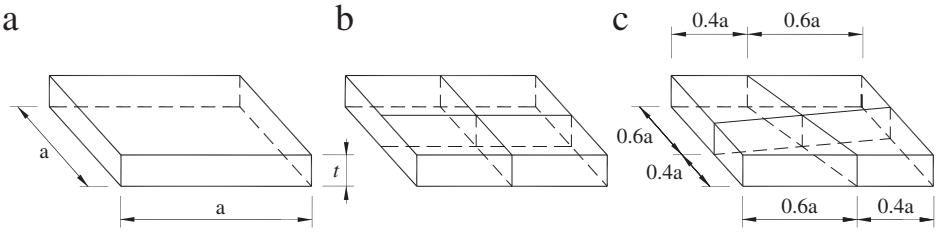

Fig. 2. Meshes of square plates ((a) mesh I; (b) mesh II; (c) mesh III).

Table 1
Frequency parameters $\lambda = (\omega a^2/\pi^2)\sqrt{\rho t/D_0}$ for a cantilever square plate ($t/a = 0.5$)

Method		DOFs	Mode number							
			1	2	3	4	5	6	7	8
Mesh I	$p = 1$	54	0.3255	0.4775	0.5783	1.1058	1.2924	1.3005	1.7993	1.8121
	$p = 2$	144	0.3027	0.4511	0.5331	1.0741	1.1768	1.2110	1.5526	1.6490
	$p = 3$	300	0.2997	0.4476	0.5292	1.0690	1.1151	1.1901	1.4898	1.5294
	$p = 4$	540	0.2985	0.4460	0.5271	1.0675	1.1105	1.1872	1.4816	1.5241
	$p = 5$	882	0.2980	0.4455	0.5267	1.0667	1.1095	1.1868	1.4805	1.5225
	$p = 6$	1344	0.2977	0.4451	0.5264	1.0663	1.1090	1.1865	1.4798	1.5224
Mesh II	$p = 1$	180	0.3073	0.4524	0.5495	1.0751	1.1806	1.2081	1.5731	1.6207
	$p = 2$	504	0.2993	0.4468	0.5285	1.0684	1.1150	1.1885	1.4879	1.5275
	$p = 3$	1080	0.2982	0.4455	0.5271	1.0668	1.1108	1.1868	1.4818	1.5231
	$p = 4$	1980	0.2973	0.4445	0.5263	1.0654	1.1087	1.1863	1.4797	1.5223
Mesh III	$p = 1$	180	0.3074	0.4523	0.5496	1.0749	1.1811	1.2095	1.5768	1.6225
	$p = 2$	504	0.2993	0.4468	0.5285	1.0684	1.1153	1.1887	1.4886	1.5280
	$p = 3$	1080	0.2982	0.4455	0.5271	1.0669	1.1108	1.1868	1.4819	1.5231
	$p = 4$	1980	0.2977	0.4451	0.5265	1.0663	1.1091	1.1865	1.4799	1.5224
LFE $6 \times 6 \times 3$		504	0.3107	0.4542	0.5442	1.0777	1.1863	1.2207	1.5695	1.6222
LFE $8 \times 8 \times 4$		1080	0.3056	0.4507	0.5373	1.0733	1.1553	1.2065	1.5338	1.5807
LFE $10 \times 10 \times 5$		1980	0.3030	0.4489	0.5338	1.0710	1.1397	1.1996	1.5158	1.5604
LFE $20 \times 20 \times 10$		13,860	0.2990	0.4460	0.5283	1.0674	1.1170	1.1898	1.4893	1.5322
Leissa et al. [12]			0.2996	0.4469	0.5279	1.0689	1.1144	1.1882	1.4863	1.5253
Liew et al. [13]			0.2976	0.4449	0.5263	1.0687	1.1087	1.1863	1.4795	1.5222

with $D_0 = Et^3/[12(1-\nu^2)]$ are compared with those presented by Leissa et al. [12] and Liew et al. [13] in Table 1. It can be found that very fast monotonic convergence is possible with the increasing number of hierarchical terms, and the present solutions are in good agreement with the existing results especially those of Liew et al. [13]. Comparison with the solutions of the LFE is also carried out in the table. The present element produces much more accurate natural frequencies than the LFE for the same number of DOFs. With one present square hierarchical element, the first eight frequencies with only 882 DOFs ($p = 5$) are more accurate than those of LFE with 13860 DOFs, that is to say, it needs only 6.4% DOFs compared with the LFE to obtain same accurate solutions!

Many published numerical cases of simply supported (*S*–*S*–*S*–*S*) square plates were carried out based on the 3-D elastic theory [12,14,15,16]. To compare with those available solutions, the *S*–*S*–*S*–*S* square plates meshed by four present 3-D hierarchical elements (see Fig. 2(c)) are analyzed. The frequency parameters λ of the first eight modes are listed in Table 2 along with the existing 3-D solutions. It is noted that there is an obvious typographical error in Ref. [16]. The value of the first mode for $t/b = 0.2$ was given as 1.7558 when it should be 1.7758. From the table, one can observe that the present solutions are in excellent agreement with the other 3-D results.

Table 2
Frequency parameters $\lambda = (\omega a^2/\pi^2)\sqrt{\rho t/D_0}$ for simply supported square plates

t/a	Method	Mode number							
		1	2	3	4	5	6	7	8
0.1	3-D DQ solutios [15]	1.9342	4.6250	4.6250	6.5234	6.5234	7.1064	8.6932	8.6932
	3-D Ritz solutios [12]	1.9342	4.6222	4.6222	6.5234	6.5234	7.1030	8.6617	8.6617
	3-D Ritz solutios [16]	1.9342	4.6222	4.6222	6.5234	6.5234	7.1030	8.6617	8.6617
	Present FE solutions	1.9342	4.6225	4.6225	6.5234	6.5234	7.1035	8.6687	8.6687
0.2	3-D DQ solutios [15]	1.7758	3.2617	3.2617	3.8999	3.8999	4.6127	5.6533	6.5236
	3-D Ritz solutios [12]	1.7758	3.2617	3.2617	3.8991	3.8991	4.6127	5.6524	6.5234
	3-D Ritz solutios [16]	1.7758	3.2617	3.2617	3.8991	3.8991	4.6128	5.6524	6.5234
	Present FE solutions	1.7758	3.2617	3.2617	3.8992	3.8992	4.6127	5.6526	6.5235
0.5	3-D Ritz solutios [12]	1.2590	1.3047	1.3047	1.8451	2.3312	2.3312	2.6094	2.6094
	3-D Ritz solutios [16]	1.2590	1.3047	1.3047	1.8451	2.3312	2.3312	2.6094	2.6094
	Present FE solutions	1.2590	1.3047	1.3047	1.8451	2.3312	2.3312	2.6094	2.6094

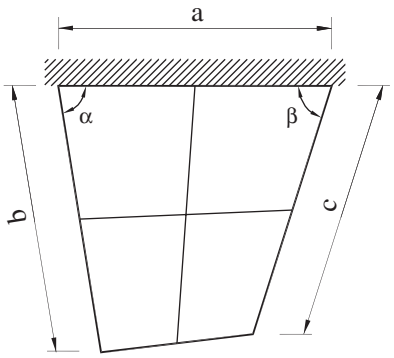

Fig. 3. Mesh of cantilever quadrilateral plate.

3.2. Vibration analysis of cantilever quadrilateral plates

Four present 3-D hierarchical elements are used to analyze the cantilever quadrilateral plates as shown in Fig. 3. One can vary the parameters α, β, a, b and c to change the shape of the plate. With various values of α, β, b/a, c/a and t/a, the frequency parameters λ of the first eight modes are shown in Table 3. Since the present element can produce very accurate natural frequencies as validated above, the results in Table 3 can be served as the benchmark data for the other numerical methods.

3.3. Vibration analysis of fully clamped regular polygonal plates

Most studies for the free vibration analysis of polygonal plates are based on the point matching method, the collocation method, the Ritz method and so on. The considerable accurate natural frequencies of the polygonal moderately thick plates can be also obtained using the HFEM just by assembling the quadrilateral elements based on the Mindlin plate theory [4]. The present 3-D element is used to analyze the polygonal thick plates in this paper. For the simplicity of computation, the polygonal plates with only fully clamped boundary conditions are considered here. The p-version meshes of the triangular, square, pentagonal and hexagonal plates are shown in Fig. 4. The same circumscribing radius of these polygons is R. With different ratios of t/R, their frequency parameters $\Omega = (4\omega R^2/\pi^2)\sqrt{\rho t/D_0}$ of the first eight modes are presented in Table 4. A common value of the additional hierarchical terms $p = 4$ is used in the computation. From Table 4, it can be found that the solutions of the present hierarchical element are in excellent agreement with the 3-D results

Table 3
Frequency parameters $\lambda = (\omega a^2/\pi^2)\sqrt{\rho t/D_0}$ for cantilever quadrilateral plates

t/a	α (deg.)	β (deg.)	b/a	c/a	Mode number							
					1	2	3	4	5	6	7	8
0.1	60	60	0.866	0.866	0.9533	3.2142	4.0196	4.7811	7.8541	8.3785	9.0683	9.4938
	60	120	0.866	0.866	0.5279	1.0857	2.7336	2.7766	3.1098	4.4311	5.2254	5.7016
	90	60	1	0.866	0.5047	1.5619	2.6124	2.9364	4.0188	5.7662	6.2819	6.6147
	90	120	1	0.866	0.3930	0.6573	1.5667	2.2345	2.3944	2.9513	3.4564	4.3359
0.2	60	60	0.866	0.866	0.8954	2.3933	2.6212	3.2776	4.5398	4.9062	5.7827	6.2625
	60	120	0.866	0.866	0.5050	0.9783	1.3908	2.3824	2.5283	2.8523	3.5691	3.6653
	90	60	1	0.866	0.4866	1.3730	1.4701	2.2147	3.1429	3.3318	3.6388	4.5324
	90	120	1	0.866	0.3809	0.6052	1.1191	1.4172	2.0561	2.4374	2.5967	2.8847
0.5	60	60	0.866	0.866	0.6893	0.9607	1.3428	1.8174	1.8185	1.9581	2.5449	3.1677
	60	120	0.866	0.866	0.4111	0.5590	0.6781	1.1426	1.3219	1.4687	1.5502	1.8908
	90	60	1	0.866	0.4079	0.5904	0.8466	1.2586	1.2904	1.4560	1.9119	2.2521
	90	120	1	0.866	0.3262	0.4471	0.4497	1.0047	1.0426	1.1548	1.2207	1.3700

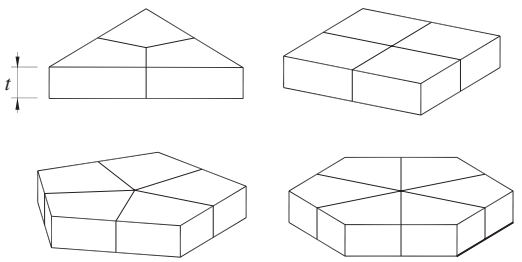

Fig. 4. Meshes of regular polygonal plates.

computed by the Ritz method [17]. Refs. [4,18] are based on the Mindlin plate theory, and their solutions are a little on the lower side than the 3-D ones of the present method and the Ritz method [17]. It should be noted that the in-plane vibration modes are not listed in Refs. [4,18].

3.4. Free vibration of a space structure

A space concrete structure is shown in Fig. 5. The structure is analyzed by the present hierarchical element and the LFE with different meshes (see Fig. 5(c) and (d)), respectively. The following parameters are used in the computation: the Young's modulus $E = 30 \times 10^9$ Pa, the density $\rho = 2500\,\mathrm{kg/m^3}$ and the Possion's ratio $v = 0.3$. For the coarse mesh with different hierarchical terms of the present element and the fine mesh of the LFE, their lowest eight natural frequencies are listed in Table 5. It also can be found that the frequencies predicted by the present element are more accurate than those of the LFE. This numerical case validates the proposed hierarchical element for the 3-D vibration analysis of space structures.

4. Experimental study

An experiment is set to study the free decaying vibration responses of a cantilever moderately thick plate. The tested acrylic plate and its numerical model are depicted in Fig. 6(a) and (b), respectively. Two accelerometers are installed at A and C. In the numerical analysis, each accelerometer is modeled as a mass (0.035 kg) attached at A or C. Other parameters of the plate are: the thickness of the plate $t = 0.01$ m, Young's modulus $E = 3.7 \times 10^9$ Pa, the density $\rho = 1400\,\mathrm{kg/m^3}$ and Possion's ratio $v = 0.33$. There are 40 hierarchical elements used in the analysis (see Fig. 6(b)).

Table 4
Frequency parameters $\Omega = (4\omega R^2/\pi^2)\sqrt{\rho t/D_0}$ for fully clamped polygonal plates

Polygon	$t/(2R)$	Method	Mode number							
			1	2	3	4	5	6	7	8
Triangle	$\sqrt{3}/20$	Present	10.70	18.26	18.26	26.14	26.40	26.40	27.28	27.28
		Ref. [4]	10.53	17.93	17.93	25.55	—	—	26.70	26.70
		Ref. [18]	10.51	17.87	17.87	25.48	—	—	26.61	26.61
	$\sqrt{3}/10$	Present	7.526	11.88	11.88	13.22	13.22	16.33	16.40	16.88
		Ref. [4]	7.321	11.52	11.52	—	—	—	15.78	16.31
	$\sqrt{3}/4$	Present	3.644	5.296	5.296	5.420	5.420	6.443	6.443	6.501
Square	$\sqrt{2}/20$	Present	6.677	12.75	12.75	17.89	21.13	21.33	25.08	25.08
		Ref. [17]	6.643	12.69	12.69	17.81	21.00	21.20	25.04	25.04
		Ref. [4]	6.591	12.57	12.57	17.62	20.76	20.96	—	—
		Ref. [18]	6.591	12.57	12.57	17.62	20.76	20.96	—	—
	$\sqrt{2}/10$	Present	5.469	9.568	9.568	12.56	12.56	12.86	14.68	14.88
		Ref. [18]	5.452	9.545	9.545	12.55	12.55	12.84	14.65	14.85
		Ref. [4]	5.375	9.381	9.381	—	—	12.60	14.35	14.55
	$\sqrt{2}/4$	Present	3.104	4.884	4.884	5.034	5.034	5.953	6.391	7.162
		Ref. [17]	3.099	4.879	4.879	5.030	5.030	5.953	6.385	7.155
Pentagon	0.1	Present	5.081	9.552	9.552	14.20	14.20	15.89	16.07	16.07
		Ref. [4]	5.014	9.410	9.410	13.97	13.97	15.61	—	—
	0.2	Present	3.928	6.687	6.687	8.053	8.053	9.397	9.418	9.418
	0.5	Present	2.058	3.202	3.202	3.225	3.225	3.76	4.211	4.211
Hexagon	0.1	Present	4.608	8.747	8.747	13.16	13.16	14.71	15.29	15.29
		Ref. [4]	4.550	8.624	8.624	12.95	12.95	14.46	—	—
	0.2	Present	3.628	6.232	6.232	7.663	7.663	8.846	8.846	8.888
	0.5	Present	1.936	3.023	3.023	3.069	3.069	3.556	4.086	4.086

In order to compare the free decaying vibration responses computed by the present hierarchical element with the experimental data, the damping ratios of the structure should be identified firstly. The Rayleigh damping [19] is adopted in the finite-element model and the damping ratios of the first two modes are identified using the continuous wavelet transform (CWT) as follows [20–22].

Instead of a linear free MDOF system with N DOFs, N uncoupled equations similar to a single DOF system are obtained

$$m_i\ddot{x}_i(t) + c_i\dot{x}_i(t) + k_i x_i(t) = 0. \tag{10}$$

The impulse response of each uncoupled system can be given in general form as

$$x_i(t) = A_{i0}\mathrm{e}^{-\xi_i\omega_i t}\cos(\sqrt{1-\xi_i}\omega_i t + \psi_i), \tag{11}$$

where ω_i, ξ_i, A_i and ψ_i are the natural frequency, damping ratio, residue magnitude and phase lag of the ith mode. If the damping is small, the impulse response can be considered asymptotic and the amplitude of the signal is

$$A_i(t) = A_{i0}\mathrm{e}^{-\xi_i\omega_i t}. \tag{12}$$

Substituting Eqs. (12) into Eq. (11), developing the amplitude using Taylor's series and neglecting terms of the order of one and superior to one, the wavelet transform of the damped signal can be rewritten as

$$(Wf)(a,b) \approx A_i(b)\Psi^*(a\omega_{di})\mathrm{e}^{\mathrm{j}\varphi_i(b)}, \tag{13}$$

where the damped frequencies $\omega_{di} = \sqrt{1-\xi_i}\omega_i$. The modulus of Eq. (13) is given by

$$|(Wf)(a,b)| \approx A_i(b)|\Psi^*(a\omega_{di})|. \tag{14}$$

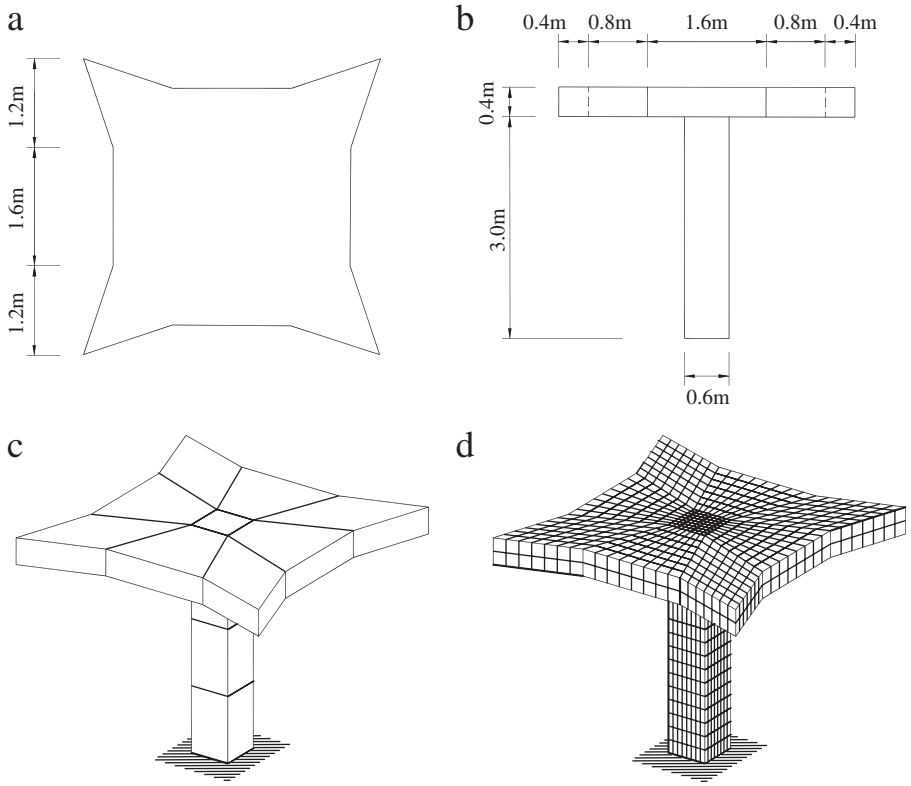

Fig. 5. Geometric size and meshes for the free vibration of a space structure ((a) top view of the structure; (b) front view of the structure; (c) p-mesh with present 3-D hierarchical element; (d) h-mesh with linear finite element).

Table 5
Natural frequencies ω (Hz) for the space structure

Method	DOFs	Mode number							
		1	2	3	4	5	6	7	8
Present ($p=1$)	576	7.170	7.170	9.232	30.70	30.70	56.18	62.13	128.7
Present ($p=2$)	1584	7.104	7.104	8.494	29.11	29.11	53.78	60.49	121.7
Present ($p=3$)	3360	7.086	7.086	8.475	28.77	28.77	53.30	59.97	121.1
LFEM	8163	7.259	7.259	8.545	29.82	29.82	55.62	61.74	127.3

For a given value of dilation a_0, from Eqs. (11) and (14), applying logarithm to Eq. (14) gives

$$\ln |(Wf)(a_0,b)| \approx -\xi_i\omega_i b + \ln[A_{i0}|\Psi^*(\pm\sqrt{1-\xi_i}\mathrm{j}\omega_i a_0)|]. \tag{15}$$

The damping ratio of the ith mode is obtained from Eq. (15). With the Rayleigh damping matrix $\mathbf{C}$ from the damping ratios of the first two modes [19], the free damped vibration equation is given by

$$\mathbf{M}\ddot{\mathbf{V}}(t) + \mathbf{C}\dot{\mathbf{V}}(t) + \mathbf{K}\mathbf{V}(t) = \{0\}, \tag{16}$$

where $\mathbf{V}(t)$ is the vectors of displacement.

A string is used to generate a 0.01 m transverse displacement at A and then cut it off to achieve the free decay responses at A and C. The free decay acceleration signal at A is low-pass filtered with a 100 Hz cutoff, and its power spectral density is shown in Fig. 7. Performing the complex Morlet wavelet transform (command *cmor1-1* in the MATLAB) to the free decay acceleration signal, the contour plot of the modulus expressing the

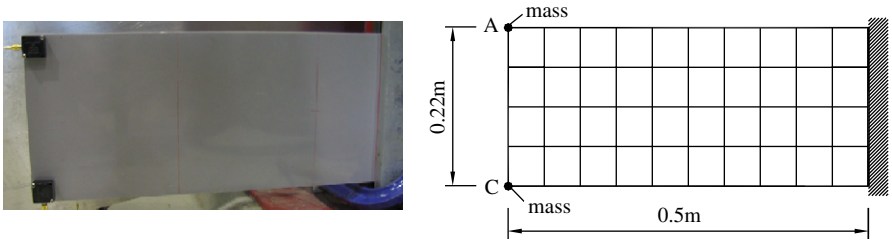

Fig. 6. Experimental setup.

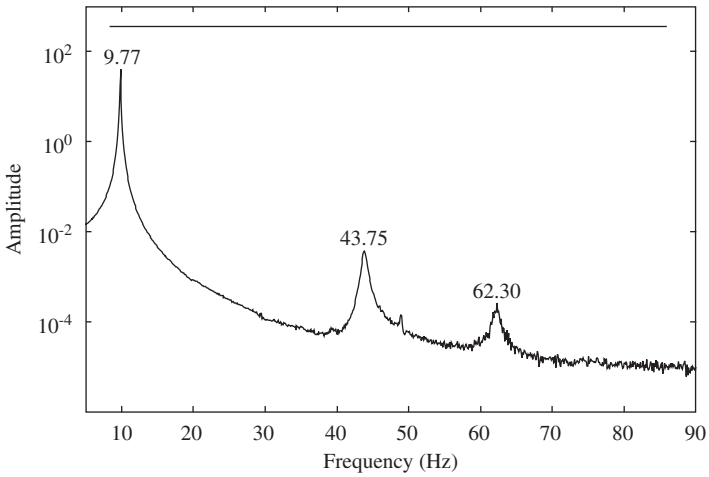

Fig. 7. Power spectral density of the free decaying signal.

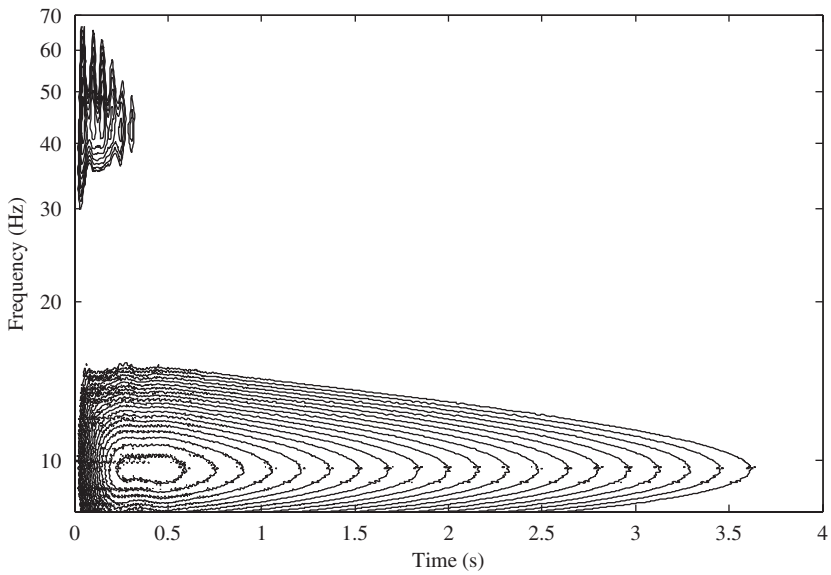

Fig. 8. Contour plot of the first two modes.

time–frequency characteristics of the signal is presented in Fig. 8. In order to increase the visibility of the picture, if the modulus of the wavelet transform is negative, the amplitude value is not represented on the plot. The first two modes of the structure are shown in the plot, and response of the second mode decays rapidly.

With band-pass filtered from 5 to 20 and from 35 to 55 Hz, respectively, the free decay responses of the first two modes at A are shown in Fig. 9(a) and (b). Also, performing CWT with command *cmor1-1* to both signals, the peak envelopes of the transformed signals are shown in Fig. 10. By linear least square, the damped frequencies can be read from Fig. 10(a) and the damping ratios of the first two modes are obtained by calculating the slopes of the two lines in Fig. 10(b). More details about the identification of vibration parameters can refer to Refs. [20–22]. These results along with the natural frequencies computed by the present hierarchical element are presented in Table 6.

With the identified damping ratios of the first two modes, the free decay acceleration responses of the structure can be computed by Eq. (16) and the Newmark linear acceleration method [19]. Compared with the experimental data, the free decay acceleration responses at A and C are shown in Fig. 11. From the pictures, it

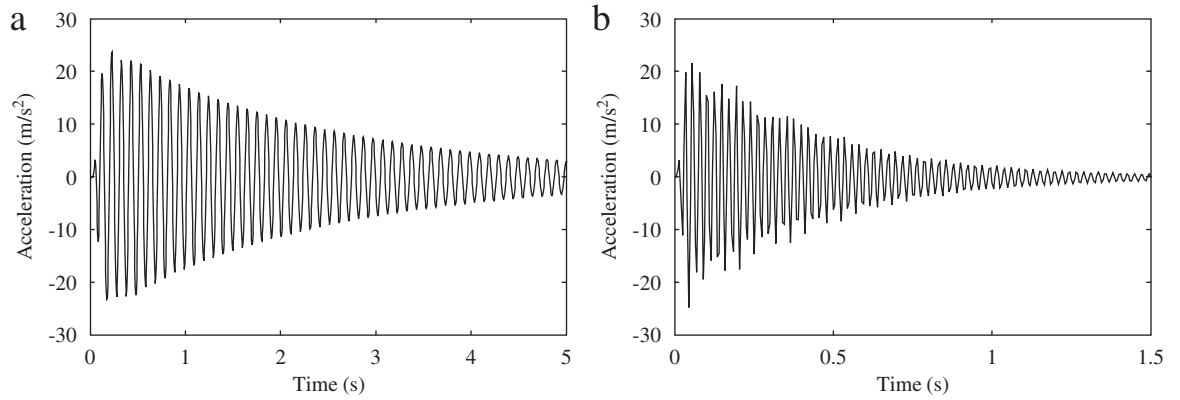

Fig. 9. Impulse responses of the first two modes ((a) first mode; (b) second mode).

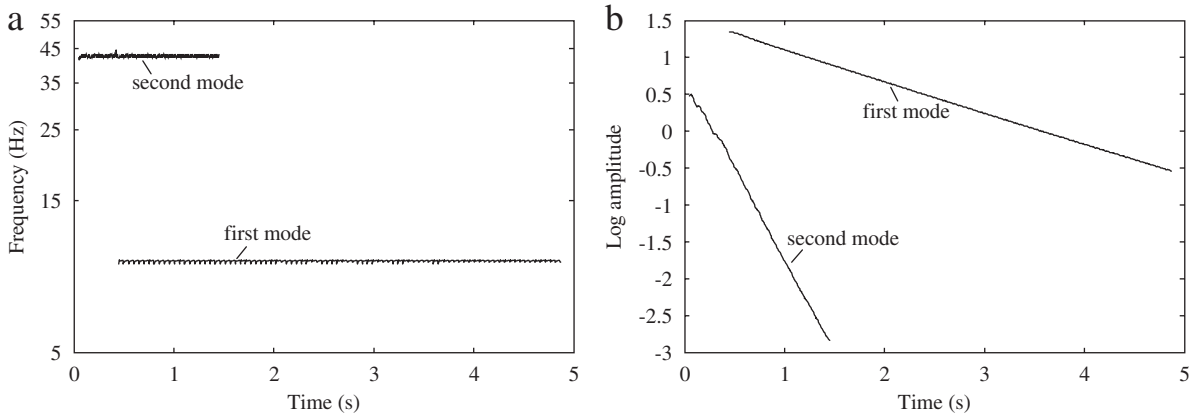

Fig. 10. Peak envelopes of wavelet transformed signal ((a) time–frequency plot; (b) time–amplitude logarithmic plot).

Table 6
Natural frequencies (Hz) and damping ratios of the cantilever acrylic plate

Method	Natural frequency (Hz)			Damping ratio (%)	
	1	2	3	1	2
p-version FEM ($p = 1$)	10.01	44.27	63.45	—	—
p-version FEM ($p = 2$)	9.94	43.82	62.62	—	—
Fast Fourier transform (FFT)	9.77	43.75	62.30	—	—
Continuous wavelet transform (CWT)	9.67	42.55	—	0.708	0.923

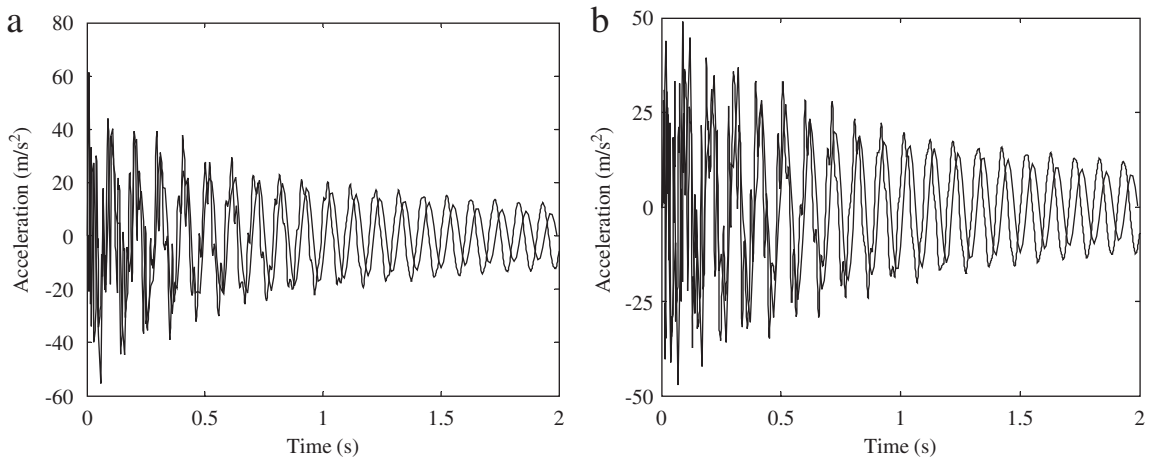

Fig. 11. Comparison between the acceleration responses computed by the present element and the experimental ones (solid line: responses computed by the present element; dashed line: experimental signals).

can be found that the signals computed by the present element are in good agreement with the experimental ones. It should be noted that there are some high-frequency noises in the experimental data, and only one hierarchical term is used in the analysis. If the influence of noise is eliminated and more hierarchical terms are used, the present solutions will be in better agreement with the experiment.

5. Conclusions

A 3-D *p*-version arbitrary quadrilateral plate element is presented in this paper. It can be applied to the vibration analysis of plates with complicated shapes. With the same number of DOFs, the present element produces much higher accurate modes than the linear 3-D finite element.

Two numerical examples, a cantilever square plate with different hierarchical terms and simply supported square plates with different thickness, are used to study the convergence rate. The results are compared with available solutions including those of other 3-D methods. The results show that the convergence rate of the proposed element is very fast with respect to the number of hierarchical terms. Its predicted natural frequencies are in excellent agreement with those of 3-D differential quadrature method and 3-D Ritz method. To show the versatility of the element, the quadrilateral and polygonal plates with different thickness are also analyzed. Furthermore, the numerical case of a space structure shows that the present element is efficient for the vibration analysis of 3-D space structures. A simple experiment is installed to study the proposed element for the analysis of free vibration responses. The CWT is used to determine the damped frequencies and damping ratios. The responses computed by the present element, based on the Rayleigh damping model and Newmark linear acceleration method, are in good agreement with the experimental ones.

Acknowledgment

The research is supported by the Hong Kong Research Grant Council #116105 and National Natural Science Foundation of China: 50608062.

Appendix A. Coefficients of stiffness and mass matrices

If $m = 3\{l+[(j-1)(p_x+2)+k-1]\ (p_y+2)\}-2$ and $n = 3\{t+[(r-1)(p_x+2)+s-1]\ (p_y+2)\}-2$,

$$K^e_{m,n} = \int_{-1}^{1}\int_{-1}^{1}[(F^2+v_2C^2)t^4W_{1010}Wzz_{00}+(-FD-v_2CA)t^4W_{1001}Wzz_{00}+(-DF-v_2AC)t^4 \times W_{0110}Wzz_{00}+(D^2+v_2A^2)t^4W_{0101}Wzz_{00}+16|\mathbf{J}|^2v_2W_{0000}Wzz_{11}]/(4t^2|\mathbf{J}|)\,\mathrm{d}\xi\,\mathrm{d}\eta;$$

else if $m = 3\{l+[(j-1)(p_x+2)+k-1]\ (p_y+2)\}-2$ and $n = 3\{t+[(r-1)(p_x+2)+s-1]\ (p_y+2)\}-1$,

$$K^e_{m,n} = \int_{-1}^{1}\int_{-1}^{1}[-(v_1CF+v_2CF)W_{1010}Wzz_{00}+(v_1FA+v_2CD)W_{1001}Wzz_{00} + (v_1DC+v_2AF)W_{0110}Wzz_{00}-(v_1AD+v_2AD)W_{0101}Wzz_{00}]t^2/(4|\mathbf{J}|)\,\mathrm{d}\xi\,\mathrm{d}\eta;$$

else if $m = 3\{l+[(j-1)(p_x+2)+k-1]\ (p_y+2)\}-2$ and $n = 3\{t+[(r-1)(p_x+2)+s-1]\ (p_y+2)\}$,

$$\mathbf{K}^e_{m,n} = \int_{-1}^{1}\int_{-1}^{1}[v_1FW_{1000}Wzz_{01}-v_1DW_{0100}Wzz_{01}+v_2FW_{0010}Wzz_{10} - v_2DW_{0001}Wzz_{10}]\,\mathrm{d}\xi\,\mathrm{d}\eta;$$

else if $m = 3\{l+[(j-1)(p_x+2)+k-1]\ (p_y+2)\}-1$ and $n = 3\{t+[(r-1)(p_x+2)+s-1]\ (p_y+2)\}-2$,

$$\mathbf{K}^e_{m,n} = \int_{-1}^{1}\int_{-1}^{1}[-(v_1CF+v_2CF)W_{1010}Wzz_{00}+(v_1CD+v_2FA)W_{1001}Wzz_{00} + (v_1AF+v_2DC)W_{0110}Wzz_{00}-(v_1AD+v_2AD)W_{0101}Wzz_{00}]t_2/(4|\mathbf{J}|)\,\mathrm{d}\xi\,\mathrm{d}\eta;$$

else if $m = 3\{l+[(j-1)(p_x+2)+k-1]\ (p_y+2)\}-1$ and $n = 3\{t+[(r-1)(p_x+2)+s-1]\ (p_y+2)\}-1$,

$$\mathbf{K}^e_{m,n} = \int_{-1}^{1}\int_{-1}^{1}[(C^2+v_2F^2)t^4W_{1010}Wzz_{00}+(-CA-v_2FD)t^4W_{1001}Wzz_{00}+(-AC-v_2DF)t^4 \times W_{0110}Wzz_{00}+(A^2+v_2D^2)t^4W_{0101}Wzz_{00}+16|\mathbf{J}|^2v_2W_{0000}Wzz_{11}]/(4t^2|\mathbf{J}|)\,\mathrm{d}\xi\,\mathrm{d}\eta;$$

else if $m = 3\{l+[(j-1)(p_x+2)+k-1]\ (p_y+2)\}-1$ and $n = 3\{t+[(r-1)(p_x+2)+s-1]\ (p_y+2)\}$,

$$\mathbf{K}^e_{m,n} = \int_{-1}^{1}\int_{-1}^{1}[-v_1CW_{1000}Wzz_{01}+v_1AW_{0100}Wzz_{01}-v_2CW_{0010}Wzz_{10} + v_2AW_{0001}Wzz_{10}]\,\mathrm{d}\xi\,\mathrm{d}\eta;$$

else if $m = 3\{l+[(j-1)(p_x+2)+k-1]\ (p_y+2)\}$ and $n = 3\{t+[(r-1)(p_x+2)+s-1]\ (p_y+2)\}-2$,

$$\mathbf{K}^e_{m,n} = \int_{-1}^{1}\int_{-1}^{1}[v_1FW_{0010}Wzz_{10}-v_1DW_{0001}Wzz_{10}+v_2FW_{1000}Wzz_{01} -v_2DW_{0100}Wzz_{01}]\,\mathrm{d}\xi\,\mathrm{d}\eta;$$

else if $m = 3\{l+[(j-1)(p_x+2)+k-1]\ (p_y+2)\}$ and $n = 3\{t+[(r-1)(p_x+2)+s-1]\ (p_y+2)\}-1$,

$$\mathbf{K}^e_{m,n} = \int_{-1}^{1}\int_{-1}^{1}[-v_1CW_{0010}Wzz_{10}+v_1AW_{0001}Wzz_{10}-v_2CW_{1000}Wzz_{01} + v_2AW_{0100}Wzz_{01}]\,\mathrm{d}\xi\,\mathrm{d}\eta;$$

else if $m = 3\{l+[(j-1)(p_x+2)+k-1]\ (p_y+2)\}$ and $n = 3\{t+[(r-1)(p_x+2)+s-1]\ (p_y+2)\}$,

$$\mathbf{K}^e_{m,n} = \int_{-1}^{1}\int_{-1}^{1}[16|\mathbf{J}|^2W_{0000}Wzz_{11}+(C^2+F^2)t^4v_2W_{1010}Wzz_{00}-(CA+FD)t^4v_2W_{1001}Wzz_{00} + (-AC-DF)t^4v_2W_{0110}Wzz_{00}+(A^2+D^2)t^4v_2W_{0101}Wzz_{00}]/(4t^2|\mathbf{J}|)\,\mathrm{d}\xi\,\mathrm{d}\eta.$$

If $m = 3\{l+[(j-1)(p_x+2)+k-1]\ (p_y+2)\}-2$ and $n = 3\{t+[(r-1)(p_x+2)+s-1]\ (p_y+2)\}-2$,
or $3\{l+[(j-1)(p_x+2)+k-1]\ (p_y+2)\}-1$ and $n = 3\{t+[(r-1)(p_x+2)+s-1]\ (p_y+2)\}-1$,
or $3\{l+[(j-1)(p_x+2)+k-1]\ (p_y+2)\}$ and $n = 3\{t+[(r-1)(p_x+2)+s-1]\ (p_y+2)\}$,

$$\mathbf{M}^e_{m,n} = \int_{-1}^{1}\int_{-1}^{1}[|\mathbf{J}|W_{0000}Wzz_{00}]\,\mathrm{d}\xi\,\mathrm{d}\eta;$$

else then

$$\mathbf{M}^e_{m,n} = 0.$$

Here $A = a + b\eta$, $C = c + b\xi$, $D = d + e\eta$, $F = f + e\xi$, $v_1 = v/(1-\nu)$ and $v_2 = (1-2v)/[2(1-v)]$ with v being the Poisson's ratio and

$$W_{\alpha\beta\chi\delta} = f_j^{\alpha}(\xi) f_k^{\beta}(\eta) f_r^{\chi}(\xi) f_s^{\delta}(\eta),$$

$$Wzz_{\alpha\beta} = f_l^{\alpha}(\zeta) f_t^{\beta}(\zeta),$$

with $j, r = 1, 2, \ldots, p_x + 2$; $k, s = 1, 2, \ldots, p_y + 2$; $l, t = 1, 2, \ldots, p_z + 2$; and the superscripts α, β, χ, δ (α, β, χ, $\delta = 0$, 1) denote the order of the derivatives.

References

[1] N.S. Bardell, Free vibration analysis of a flat plate using the hierarchical finite element method, *Journal of Sound and Vibration* 151 (1991) 263–289.

[2] N.S. Bardell, The free vibration of skew plates using the hierarchical finite element method, *Computers & Structures* 45 (1992) 841–874.

[3] O. Beslin, J. Nicolas, Hierarchical functions set for predicting very high order plate bending modes with any boundary conditions, *Journal of Sound Vibration* 202 (1997) 633–655.

[4] B. Zhu, A.Y.T. Leung, Vibration analyses of Mindlin plates by quadrilateral *p*-version elements, *Proceedings of WCCM VI (CD Rom)*, Beijing, China, 2004.

[5] O. Attia, A.E. Zafrany, A high-order shear element for nonlinear vibration analysis of composite layered plates and shells, *International Journal of Mechanical Sciences* 41 (1999) 461–486.

[6] O.C. Zienkiewicz, R.L. Taylor, *The Finite Element Method*, fourth ed., McGraw-Hill, New York, 1989.

[7] A. Houmat, Three-dimensional hierarchical finite element free vibration analysis of annular sector plates, *Journal of Sound and Vibration* 276 (2004) 181–193.

[8] A.Y.T. Leung, B. Zhu, Hexahedral Fourier *p*-elements for vibration of prismatic solids, *International Journal of Structural Stability and Dynamic* 4 (2004) 125–138.

[9] A.Y.T. Leung, B. Zhu, Comments on "Free Vibration of Skew Mindlin Plates by *p*-version of F.E.M.", *Journal of Sound and Vibration* 278 (2004) 699–703.

[10] A.Y.T. Leung, *Dynamic Stiffness and Substructures*, Springer, London, 1993.

[11] A. Houmat, A triangular Fourier *p*-element for the analysis of membrane vibrations, *Journal of Sound and Vibration* 230 (2000) 31–43.

[12] A.W. Leissa, Z.D. Zhang, On the three-dimensional vibrations of the cantilevered rectangular parallelepiped, *Journal of the Acoustical Society of America* 73 (1983) 2013–2021.

[13] K.M. Liew, K.C. Hung, M.K. Lim, A continuum three-dimensional vibration analysis of thick rectangular plates, *International Journal of Solids and Structures* 30 (1993) 3357–3379.

[14] C.M. Wang, J.N. Reddy, K.H. Lee, *Shear Deformable Beams and Plates*, Elsevier, Oxford, UK, 2000.

[15] M. Malik, C.W. Bert, Three-dimensional elasticity solutions for free vibrations of rectangular plates by the differential quadrature method, *International Journal of Solids and Structures* 35 (1998) 299–319.

[16] D. Zhou, Y.K. Cheng, F.T.K. Au, S.H. Lo, Three-dimensional vibration analysis of thick rectangular plates using Chebyshev polynomial and Ritz method, *International Journal of Solids and Structures* 39 (2002) 6339–6353.

[17] K.M. Liew, K.C. Hung, M.K. Lim, Three-dimensional vibration of rectangular plates: variance of simple support conditions and influence of in-plane inertia, *International Journal of Solids and Structures* 31 (1994) 3233–3247.

[18] K.M. Liew, C.M. Wang, Y. Xiang, S. Kitipornchai, *Vibration of Mindlin Plates*, Elsevier, Oxford, UK, 1998.

[19] R.W. Clough, J. Penzien, *Dynamics of Structures*, second ed., McGraw-Hill, New York, 1993.

[20] W.J. Staszewski, Identification of damping in MDOF systems using time-scale decomposition, *Journal of Sound and Vibration* 203 (1997) 283–305.

[21] M. Ruzzene, A. Fasana, L. Garibaldi, B. Piombo, Natural frequencies and damping identification using wavelet transform: application to real data, *Mechanical Systems and Signal processing* 11 (1997) 207–218.

[22] J. Lardies, S. Gouttebroze, Identification of modal parameters using the wavelet transform, *International Journal of Mechanical Science* 44 (2002) 2263–2283.